

This is a repository copy of *Search for Weak Side Branches in the Electromagnetic Decay Paths of the 6526-keV 10+ Isomer in 54Fe*.

White Rose Research Online URL for this paper:

<https://eprints.whiterose.ac.uk/id/eprint/205385/>

Version: Published Version

Article:

Böhm, Paul, Hrabar, Yuliia, Rudolph, Dirk et al. (20 more authors) (2023) Search for Weak Side Branches in the Electromagnetic Decay Paths of the 6526-keV 10+ Isomer in 54Fe. Atoms. 116. ISSN: 2218-2004

<https://doi.org/10.3390/atoms11090116>

Reuse

This article is distributed under the terms of the Creative Commons Attribution (CC BY) licence. This licence allows you to distribute, remix, tweak, and build upon the work, even commercially, as long as you credit the authors for the original work. More information and the full terms of the licence here:





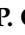







<https://creativecommons.org/licenses/>

Takedown

If you consider content in White Rose Research Online to be in breach of UK law, please notify us by emailing eprints@whiterose.ac.uk including the URL of the record and the reason for the withdrawal request.

Article

Search for Weak Side Branches in the Electromagnetic Decay Paths of the 6526-keV 10^+ Isomer in ^{54}Fe

Paul Böhm ¹, Yuliia Hrabar ¹, Dirk Rudolph ^{1,*}, Pavel Golubev ¹, Luis G. Sarmiento ¹, Helena M. Albers ², John T. Anderson ³, Michael A. Bentley ⁴, Michael P. Carpenter ³, Christopher J. Chiara ⁵, Patrick A. Copp ^{3,†}, Ulrika Forsberg ^{1,‡}, Tianheng Huang ³, Heshani Jayatissa ^{3,†}, Torben Lauritsen ³, Claus Müller-Gattermann ³, Xesus Pereira-Lopez ^{4,§}, Walter Reviol ³, Darek Seweryniak ³, Sanna Stolze ³, Sivahami Uthayakumaar ^{4,||}, Gemma L. Wilson ^{3,6,¶} and Jin Wu ^{3,**}

¹ Department of Physics, Lund University, S-22100 Lund, Sweden

² GSI Helmholtzzentrum für Schwerionenforschung, D-64291 Darmstadt, Germany

³ Physics Division, Argonne National Laboratory, Argonne, IL 60439, USA

⁴ Department of Physics, University of York, Heslington, York YO10 5DD, UK

⁵ U.S. Army Combat Capabilities Development Command Army Research Laboratory, Adelphi, MD 20783, USA

⁶ Department of Physics & Astronomy, Louisiana State University, Baton Rouge, LA 70803, USA

* Correspondence: dirk.rudolph@nuclear.lu.se

† Current address: Los Alamos National Laboratory, Los Alamos, NM 87545, USA.

‡ Current address: Studsvik Nuclear AB, 610 60 Linköping, Sweden.

§ Current address: Center for Exotic Nuclear Studies, Institute for Basic Science, Daejeon 34126, Republic of Korea.

|| Current address: Facility for Rare Isotope Beams, Michigan State University, East Lansing, MI 48824, USA.

¶ Current address: United Kingdom Atomic Energy Authority, Abingdon, Oxon OX14 3DB, UK.

** Current address: Brookhaven National Laboratory, Brookhaven, NY 11873, USA.



Citation: Böhm, P.; Hrabar, Y.; Rudolph, D.; Golubev, P.; Sarmiento, L.G.; Albers, H.M.; Anderson, J.T.; Bentley, M.A.; Carpenter, M.P.; Chiara, C.J.; et al. Search for Weak Side Branches in the Electromagnetic Decay Paths of the 6526-keV 10^+ Isomer in ^{54}Fe . *Atoms* **2023**, *11*, 116. <https://doi.org/10.3390/atoms11090116>

Academic Editor: Giuseppe Mandaglio

Received: 27 July 2023

Revised: 17 August 2023

Accepted: 22 August 2023

Published: 24 August 2023



Copyright: © 2023 by the authors. Licensee MDPI, Basel, Switzerland. This article is an open access article distributed under the terms and conditions of the Creative Commons Attribution (CC BY) license (<https://creativecommons.org/licenses/by/4.0/>).

Abstract: High-spin nuclear isomers in $N \approx Z$ nuclei between doubly magic ^{40}Ca and ^{56}Ni provide an excellent testing ground for the nuclear shell model and questions related to isospin symmetry breaking in the vicinity of the proton drip line. The purpose of the present study is to investigate the possibility of weak electromagnetic decay branches along the decay paths of the 6526-keV 10^+ isomer in ^{54}Fe . The isomer was strongly populated by means of the fusion-evaporation reaction $^{24}\text{Mg}(^{36}\text{Ar}, \alpha 2p)^{54m}\text{Fe}$. The Gammasphere array was used to detect γ -ray cascades emitted from the isomeric state. By means of $\gamma\gamma\gamma$ coincidences, weak non-yrast decay branches can be discriminated, with the isomer's half-life confirmed at $T_{1/2} = 363(4)$ ns. The yrast $6_1^+ \rightarrow 2_1^+$ $E4$ cross-over transition was interrogated. The observations are compared with shell-model calculations.

Keywords: nuclear isomer; electromagnetic transitions; nuclear shell model

1. Introduction

In the vicinity of self-conjugated $N \approx Z$ nuclei between $^{40}_{20}\text{Ca}_{20}$ and $^{56}_{28}\text{Ni}_{28}$, strongly attractive two-body matrix-elements between neutron and proton $f_{7/2}$ particles (or holes) give rise to spin-gap isomers with high angular momenta. Examples near ^{56}Ni are $I^\pi = 7^+$ in $^{54}_{27}\text{Co}_{27}$, $I^\pi = 12^+$ in $^{52}_{26}\text{Fe}_{26}$, or $I^\pi = 19/2^-$ in case of the $A = 53$ ($^{53}_{26}\text{Fe}_{27}$ and $^{53}_{27}\text{Co}_{26}$) ‘mirror isomers’, respectively. The $I^\pi = 10^+$ ‘mirror isomers’ in the $A = 54$ nuclei $^{54}_{26}\text{Fe}_{28}$ and $^{54}_{28}\text{Ni}_{26}$ are core-excited states. To first order, they arise from closely lying multiplets of states, which are based on the coupling of a respective $A = 53$ ‘mirror isomer’ with a single nucleon in the upper fp shell. In fact, energy differences between excited states in $\mathcal{N} = 3$, fp -shell mirror nuclei have been and continue to be a rich source of information on isospin symmetry breaking at or beyond the proton dripline. For background material as well as more recent developments, see, for instance, Refs. [1–7] and references therein.

For some neutron-deficient mirror partners, e.g., ^{53m}Co and ^{54m}Ni , Q values allow for intriguing competition between electromagnetic decays ($E2$ and/or $E4$), β -decay, and

proton radioactivity. In fact, the observation of a weak $\ell = 9$ proton-emission branch from the 3174-keV ^{53m}Co isomeric state into the ground state of ^{52}Fe marked the discovery of proton radioactivity in atomic nuclei in 1970 [8,9]. Interestingly, it took more than 50 years to disentangle the complete decay pattern of this isomeric state by means of a combination of Penning-trap-assisted decay spectroscopy and 4D imaging of charged-particle decays with a time-projection chamber [10]. In the same experimental campaign, both proton-emission branches of ^{54m}Ni were determined [11,12]. The new experimental results were compared to cutting-edge shell-model and barrier penetration calculations for these (very) high- ℓ protons with $\ell = 5, 7$, and 9 , all (very) far beyond the $\mathcal{N} = 3, f_{7/2}$ shell [10,11]. Further, the complete decay pattern of ^{54m}Ni allowed the derivation of reduced transition strengths, $B(E2; 10_1^+ \rightarrow 8_1^+)$ and $B(E4; 10_1^+ \rightarrow 6_1^+)$, for the two competing γ -ray transitions from ^{54m}Ni [13]. By means of a comparison with their well-known ‘mirror transitions’ in $T_z = +1$ ^{54}Fe , effective charges for $E4$ transitions near $N = Z$ ^{56}Ni could be suggested. The $B(E6; 19/2^- \rightarrow 7/2^-)$ strength in ^{53m}Fe has recently been used to study effective charges for $E6$ transitions [14].

A basic requirement for any elaborate study on isospin symmetry breaking is comprehensive knowledge of the relevant observables of the more neutron-rich partner. Here, we report on a dedicated study to complement the electromagnetic decay pattern of the well-known 6526-keV, 10^+ isomer ^{54m}Fe [15–17].

2. Experiment

The experiment was conducted at Argonne National Laboratory (ANL). A beam of $^{36}\text{Ar}^{11+}$ ions accelerated to 88 MeV was provided by the ATLAS facility. With typical intensities of ≈ 40 enA, the beam impinged on a 0.43 mg/cm^2 thick foil of 99.92% enriched ^{24}Mg . This self-supporting foil was positioned inside a vacuum chamber in the center of the Gammasphere array used for high-fold γ -ray detection purposes [18]. At the time of the experiment, Gammasphere operated with 70 Compton-suppressed Ge detectors, because the experimental set-up comprised a number of ancillary devices to detect, for instance, evaporated neutrons with the help of 32 liquid scintillator detectors [19]. These occupied the respective slots for Gammasphere modules at forward angles with respect to the beam direction. Further, a combination of the 4π CsI(Tl) array Microball [20] and two CD-type double-sided Si strip detectors (DSSD) facilitated the detection, tracking, and spectroscopy of light-charged particles such as protons, deuterons, and α particles. Information on recoiling residual nuclei entering the Fragment Mass Analyzer (FMA) [21] in a narrow cone in the beam direction and reaching its focal plane was stored as well. More information on the complete experimental set-up can be found in, for instance, Chapter 2 of Ref. [22].

For the present study on the electromagnetic decay paths of ^{54m}Fe , only Compton-suppressed $\gamma\gamma$ and $\gamma\gamma\gamma$ coincidence events from the Gammasphere array are relevant. High-spin states of ^{54}Fe are populated in the reaction $^{24}\text{Mg}(^{36}\text{Ar}, \alpha 2p)^{54}\text{Fe}$ with the majority of the yield populating the 6526-keV, 10^+ isomer ^{54m}Fe [17]. The isomer has a reported $T_{1/2} = 364(7)$ ns [15,16]. Further, for the vast majority of the events of interest, the evaporation of an α particle in the production process causes ^{54}Fe recoils to be deflected from the beam direction, such that they are implanted and stopped in Ta foils protecting the DSSDs from radiation damage. In essence, this yields a stationary radioactive source of ^{54m}Fe close to the center of the Gammasphere array. Moreover, this source is continuously produced during the experiment. It primarily emits a cascade of five $E2$ transitions with energies $E_\gamma = 146, 411, 1130, 1408$, and 3432 keV (see Figure 1 and Ref. [17]), thereby covering the typical energy range relevant for γ -ray spectroscopy experiments.

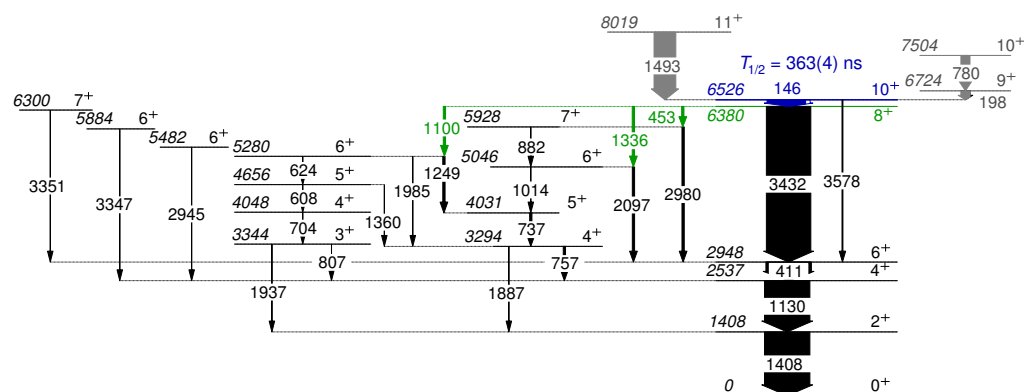


Figure 1. Partial decay scheme of ^{54}Fe [15,17] relevant for the present study. Energy labels are in keV. The thickness of the arrows scales with the relative intensities of the γ rays. Those with the thinnest arrows are not observed in the present study and are only shown for completeness. The 10^+ isomeric state as well as the $10^+ \rightarrow 8^+$ 146-keV transition, which was used to select its decay paths, are shown in blue. Known transitions populating the isomer are indicated in gray. Previously unknown transitions connecting the 6380-keV 8^+ state with side branches are marked green.

Prior to the experiment, a provisional energy calibration of the Gammasphere Ge detectors was accomplished with the help of radioactive ^{207}Bi sources. Between the present experiment, using the fusion-evaporation of $^{36}\text{Ar}+^{24}\text{Mg}$, and the second experiment of the campaign at ANL, using $^{40}\text{Ca}+^{24}\text{Mg}$ [22], extensive γ -ray energy and efficiency calibration data were taken using ^{133}Ba , ^{152}Eu , and ^{182}Ta sources placed in the center of the array.

3. Data Analysis and Results

Regarding the γ -ray analysis of the experimental campaign, a base calibration of all Ge detectors was established from the aforementioned source data [22]. Small variations of, e.g., environmental conditions during the week-long experiments can give rise to small drifts of the amplified and digitized signals of the Ge detectors. Therefore, the complete data set was divided into 10- to 12-h long sub-sets, and the gain of each individual Ge detector was re-aligned for each sub-set. For the present experiment, a semi-automated procedure was developed using the distinct 146 and 3432-keV peak positions of the ample ^{54m}Fe decays, as well as the 511-keV peak stemming primarily from β^+ -decay related positron annihilation [23].

Apart from marginal, i.e., practically non-existing contributions of the 10^+ mirror isomer in ^{54}Ni [13,15], a prompt coincidence with the 146-keV $10_1^+ \rightarrow 8_1^+$ transition highlights decays of ^{54m}Fe . To establish an appropriate choice of time differences, Δt , a correlation matrix $\Delta t(\gamma_1, \gamma_2) - E_{\gamma_2}$ was created, pre-selected with $E_{\gamma_1} = 146$ keV. As a result, the γ -ray spectrum in blue in Figure 2a shows the background-subtracted spectrum of events with $\Delta t = [-20, 60]$ ns. The spectrum is selective for γ rays depopulating the 6380-keV yrast 8_1^+ state in ^{54}Fe . In turn, the background-subtracted spectrum in grey in Figure 2a corresponds to $\Delta t = [0.15, 2.00]$ μs . It shows broad peaks of Doppler-shifted γ -ray transitions feeding the 10^+ isomer in ^{54}Fe (cf. Figure 1). In fact, selecting several of these feeding γ -ray transitions, projecting on Δt , and analyzing the resulting time spectrum, a half-life value of $T_{1/2} = 363(4)$ ns of the 10^+ isomer in ^{54}Fe can be derived. This is consistent with the literature value $T_{1/2} = 364(7)$ ns [15]. Note that the 511-keV line in Figure 2a arises from escape events following pair-production detection of the high-energy 3432-keV transition (cf. Figure 1), in combination with its single and double escape peaks.

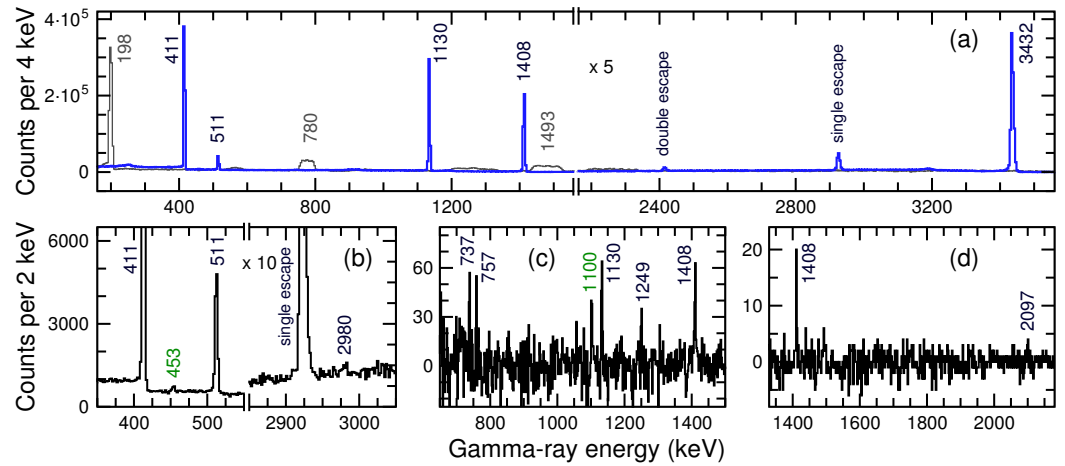


Figure 2. Gamma-ray spectra in prompt coincidence with the 146-keV transition depopulating the 10^+ isomer in ^{54}Fe . Energy labels are in keV (cf. Figure 1 and text). (a) Spectra in prompt coincidence, $\Delta t = [-20, 60]$ ns (blue, thick lines), or selecting $\Delta t = [0.15, 2.00]$ μs (gray, thin lines), i.e., providing Doppler-shifted peak structures of transitions feeding the isomer. (b) Summed spectrum in coincidence with the three transitions forming the $6^+ \rightarrow 4^+ \rightarrow 2^+ \rightarrow 0^+$ yrast cascade. (c) Summed spectrum in coincidence with the 737, 757, and 1249-keV transitions. (d) Spectrum in coincidence with the previously unobserved 1336-keV transition.

In the next step of the γ -ray analysis, an $E_{\gamma 2}$ - $E_{\gamma 3}$ $\gamma\gamma$ correlation matrix was sorted, pre-selected by $E_{\gamma 1} = 146$ keV and using a prompt time window $\Delta t(\gamma_1, \gamma_i) = [-20, 60]$ ns, $i = 2, 3$. Corresponding matrices for delayed coincidences with the 146-keV line, $\Delta t = [0.15, 2.00]$ μs , and random coincidences, $\Delta t = [-2.00, -0.50]$ μs , were created, inspected, and used for reference. A search was undertaken for (i) γ -ray transitions connecting the 6380-keV 8_1^+ state with known 6^+ and 7^+ states in ^{54}Fe , other than the 2948-keV yrast 6_1^+ level [17], and (ii) the possible 1541-keV, $6_1^+ \rightarrow 2_1^+$ $E4$ decay.

The results concerning hitherto unobserved transitions are exemplified in Figure 2b–d. They are summarized in Table 1. The experimental branching ratios are deduced from efficiency-corrected γ -ray yields of observed peaks in appropriate coincidence spectra as described in the following. First, a weak $E_{\gamma 3} = 453$ -keV line is seen in prompt coincidence with the $E_{\gamma 2} = 2980$ keV, $7_1^+ \rightarrow 6_1^+$ transition. This coincidence is seen more clearly in the spectrum shown in Figure 2b, where $E_{\gamma 3}$ in the above mentioned prompt coincidence matrix is shown, selected by the $E_{\gamma 2} = 411, 1130$, and 1408-keV transitions forming the $6_1^+ \rightarrow 4_1^+ \rightarrow 2_1^+ \rightarrow 0_1^+$ yrast cascade. Figure 2b also reveals a weak peak at 2980 keV, altogether confirming the presence of the 453-keV connection between the 6380-keV 8_1^+ and 5928-keV 7_1^+ levels, rather than that peak originating from Compton-scattered events of the main 3432-keV transition between two Ge detectors (cf. Figure 19 in Ref. [23]).

Table 1. Comparison of experimental results with predictions from shell-model calculations. See text for details. Level energies, $E_{x,i}$, and spin-parity assignments, I_i^π , are taken from Ref. [17]. Transition energies, E_γ and relative branching ratios, b_γ , are from the present study.

$E_{x,i}$ (keV)	I_i^π (\hbar)	E_γ (keV)	$E_{x,f}$ (keV)	I_f^π (\hbar)	$b_{\gamma,\text{exp}}$ (‰)	$b_{\gamma,\text{theo}}$ (‰)
6380	8_1^+	80.3(11) ¹	6300	7_2^+	<1	0.1
		452.6(5)	5928	7_1^+	3.1(4)	2.5
		496.0(17) ¹	5884	6_2^+	<1	0.0
		898.6(11) ¹	5482	6_4^+	<2	0.2
		1099.9(7)	5280	6_3^+	2.5(5)	7.3
		1335.6(10)	5046	6_5^+	1.3(5)	6.0
		3431.6(8)	2948	6_1^+	1000	1000
		411.3(2)	2537	4_1^+	1000	1000
2948	6_1^+	1539.7(10)	1408	2_1^+	<1	$4 \cdot 10^{-5}$

¹ Energy difference calculated using excitation energies listed in Ref. [17].

The γ -ray spectrum in Figure 2c represents $E_{\gamma 3}$ selected by the previously known $E_{\gamma 2} = 737, 757$, and 1249-keV transitions, which form the most intense cascade between the 5280-keV 6_3^+ and 2537-keV 4_1^+ states [17]. The spectrum shows an obvious peak at 1100 keV, next to the 1130 and 1408-keV yrast transitions. This combination assures the placement of the former between the 6380-keV 8_1^+ and 5280-keV 6_3^+ states, establishing another weak decay path parallel to the intense 3432-keV yrast transition. Next, the γ -ray spectrum in Figure 2d shows $E_{\gamma 3}$ selected by the unknown $E_{\gamma 2} = 1336$ -keV transition, placed between the 6380-keV 8_1^+ and the 5046-keV 6_2^+ states in Figure 1. The spectrum reveals weak coincidences with the cascade depopulating the 6^+ yrast level (only the 1408-keV line is shown for clarity), and also with the 2097-keV $6_2^+ \rightarrow 6_1^+$ transition. Further connections between the yrast 8_1^+ state and other yrare 6^+ or 7^+ states (cf. Figure 1) cannot be identified. Hence, only upper limits of their branching ratios can be provided in Table 1.

Similarly, also the search for a $(411 + 1130)$ keV = 1541 keV, $6^+ \rightarrow 2^+$ E4 cross-over transition proved negative. Though spectra in coincidence with the yrast $E_{\gamma 2} = 1408$ and 3432 keV transitions show a peak at $E_{\gamma 3} \approx 1540$ keV, a peak at $E_{\gamma 3} = (411 + 1408)$ keV = 1819 keV is observed with similar yield in spectra in coincidence with $E_{\gamma 2} = 1130$ and 3432 keV transitions, respectively. The presence of the ≈ 1540 keV peak (and the 1819 keV peak) is thus primarily caused by coincident summing, i.e., simultaneous hits of a single Ge-detector crystal by two γ rays stemming from the same isomeric decay event.

Note that the present results were cross-checked and found consistent with data sets from earlier experiments with Gammasphere and fusion-evaporation reactions leading to the same compound nucleus $^{60}\text{Zn}^*$ [17].

4. Discussion and Conclusions

The experimental results on branching ratios are compared with shell-model calculations in Table 1. The calculations correspond to those labeled KB3G56 in Ref. [13]. They include the isospin-breaking terms V_{CM} , V_{CIs} , V_{Cr} , and $V_{B:2}$, as outlined in Ref. [13], and are conducted in the full fp space, with up to $t = 6$ particles allowed to cross the shell gap at $N = Z = 28$. Electromagnetic transition rates are calculated using bare g factors for $M1$ transitions, effective charges $\epsilon_p = 1.15e$ and $\epsilon_n = 0.80e$ for $E2$ transitions [24], and $\epsilon_p = 1.40e$ and $\epsilon_n = 0.30e$ for $E4$ transitions [13].

Concerning the newly observed (very) weak decay branches from the 6380-keV 8_1^+ level, very good agreement is found between experiment and theory. Given that all experimental and theoretical branching ratios of interest are on the level of 1/1000 or below, the transitions predicted $b_\gamma > 1\%$ were observed, while those predicted $b_\gamma < 1\%$ correspondingly were not. The predicted $B(E4; 6_1^+ \rightarrow 2_1^+) \approx 1$ W.u. is of similar strength as the observed 3578-keV $10^+ \rightarrow 6_1^+$ decay. However, scaling its $b_\gamma \approx 2\%$ with relative $E2$ $[(146/411)^5 = 5.7 \cdot 10^{-3}]$ and $E4$ $[(1541/3578)^9 = 5.1 \cdot 10^{-4}]$ phase space factors readily explains its very low predicted branching ratio on the order of a few times 10^{-8} , which agrees with the derived experimental upper limit.

Author Contributions: D.R. prepared the proposal for the experiment at ANL with support from M.A.B., M.P.C., P.G., W.R. and D.S. The set-up at ANL was prepared by J.T.A., M.P.C., P.A.C., U.F., P.G., T.H., C.M.-G., W.R., D.R., D.S. and J.W. Software for data acquisition and data analysis was prepared by H.M.A., P.B., U.F., Y.H., T.L., D.R., L.G.S. and D.S. All authors but J.T.A. and P.B. participated in monitoring data taking during the experiment. P.B. conducted the formal analysis of the specific results on ^{54m}Fe and provided input to the figures, supervised by Y.H. and D.R. D.R. prepared the original draft and P.B., Y.H., D.R., H.M.A., M.A.B., M.P.C., C.J.C., H.J., C.M.-G., W.R. and D.S. were engaged in review and editing. All authors have read and agreed to the published version of the manuscript.

Funding: This research was funded in part by the Swedish Research Council (Vetenskapsrådet, VR 2016-3969 and VR 2022-3828), the Crafoord Foundation in Lund (Grant 20180630), the U.S. Department of Energy, Office of Science, Office of Nuclear Physics (Contract No. DE-AC02-06CH11357), and the UKRI Science and Technology Facilities Council under grant numbers ST/P003885/1 and ST/V001035/1.

Data Availability Statement: The data presented in this study are available on reasonable request from the corresponding author.

Acknowledgments: We would like to thank the ATLAS accelerator crew for their supreme efforts. This research used resources of ANL's ATLAS facility, which is a U.S. Department of Energy Office of Science User Facility. The isotope(s) used in this research were supplied by the U.S. Department of Energy Office of Science by the Isotope Program in the Office of Nuclear Physics.

Conflicts of Interest: The authors declare no conflict of interest.

Abbreviations

The following abbreviations are used in this manuscript:

ANL	Argonne National Laboratory
ATLAS	Argonne Tandem Linac Accelerator System
DSSD	Double-sided Si Strip Detector
FMA	Fragment Mass Analyzer

References

- Bentley, M.A.; Lenzi, S.M. Coulomb energy differences between high-spin states in isobaric multiplets. *Prog. Part. Nucl. Phys.* **2007**, *59*, 497–561. [\[CrossRef\]](#)
- Ekman, J.; Fahlander, C.; Rudolph, D. Mirror symmetry in the upper *fp* shell. *Mod. Phys. Lett. B* **2005**, *20*, 2977–2992. [\[CrossRef\]](#)
- Bentley, M.A.; Lenzi, S.M.; Simpson, S.A.; Diget, C.A. Isospin-breaking interactions studied through mirror energy differences. *Phys. Rev. C* **2015**, *92*, 024310. [\[CrossRef\]](#)
- Bonnard, J.; Lenzi, S.M.; Zuker, A.P. Neutron skins and halo orbits in the *sd* and *pf* shells. *Phys. Rev. Lett.* **2016**, *116*, 212501. [\[CrossRef\]](#) [\[PubMed\]](#)
- Fernández, A.; Jungclaus, A.; Doornenbal, P.; Bentley, M.A.; Lenzi, S.M.; Rudolph, D.; Browne, F.; Cortés, M.L.; Koiwai, T.; Taniuchi, R.; et al. First γ -ray spectroscopy of the $T_z = -2$ nucleus ^{56}Zn . *Phys. Lett. B* **2021**, *823*, 136784. [\[CrossRef\]](#)
- Bentley, M.A. Excited States in Isobaric Multiplets—Experimental Advances and the Shell-Model Approach. *Physics* **2022**, *4*, 995–1011. [\[CrossRef\]](#)
- Smirnova, N.A. Isospin-Symmetry Breaking within the Nuclear Shell Model: Present Status and Developments. *Physics* **2023**, *5*, 352–380. [\[CrossRef\]](#)
- Jackson, K.P.; Cardinal, C.U.; Evans, H.C.; Jelley, N.A.; Cerny, J. $^{53}\text{Co}^m$: A proton-unstable isomer. *Phys. Lett. B* **1970**, *33*, 281–283. [\[CrossRef\]](#)
- Cerny, J.; Esterl, J.E.; Gough, R.A.; Sextro, R.G. Confirmed proton radioactivity of $^{53}\text{Co}^m$. *Phys. Lett. B* **1970**, *33*, 284–286. [\[CrossRef\]](#)
- Sarmiento, L.G.; Sarmiento, L.G.; Roger, T.; Giovinazzo, J.; Brown, B.A.; Blank, B.; Rudolph, D.; Kankainen, A.; Alvarez-Pol, H.; Arokia Raj, A.; et al. Elucidating the nature of the proton radioactivity of ^{53m}Co . *Nat. Commun.* **2023**, *in press*.
- Giovinazzo, J.; Roger, T.; Blank, B.; Rudolph, D.; Brown, B.A.; Alvarez-Pol, H.; Arokia Raj, A.; Ascher, P.; Caamaño-Fresco, M.; Caceres, L.; et al. 4D-imaging of drip-line radioactivity by detecting proton emission from ^{54m}Ni pictured with ACTAR TPC. *Nat. Commun.* **2021**, *12*, 4805–4810. [\[CrossRef\]](#) [\[PubMed\]](#)
- Giovinazzo, J.; Giovinazzo, J.; Roger, T.; Blank, B.; Rudolph, D.; Alvarez-Pol, H.; Arokia Raj, A.; Ascher, P.; Caamaño-Fresco, M.; Caceres, L.; et al. Proton 3D tracking and emission time from a short-lived isomer with ACTAR-TPC. *Nucl. Instr. Meth. A* **2022**, *1042*, 167447. [\[CrossRef\]](#)
- Rudolph, D.; Blank, B.; Giovinazzo, J.; Roger, T.; Alvarez-Pol, H.; Arokia Raj, A.; Ascher, P.; Caamaño-Fresco, M.; Caceres, L.; Cox, D.M.; et al. Mirror symmetry at mass $A = 54$: $E4$ effective charges near doubly magic ^{56}Ni . *Phys. Lett. B* **2022**, *830*, 137144. [\[CrossRef\]](#)
- Palazzo, T.; Mitchell, A.J.; Lane, G.J.; Stuchbery, A.E.; Brown, B.A.; Reed, M.W.; Akber, A.; Coombes, B.J.; Dowie, J.T.H.; Eriksen, T.K.; et al. Direct Measurement of Hexacontatetrapole, $E6$ γ Decay from ^{53m}Fe . *Phys. Rev. Lett.* **2023**, *130*, 122503. [\[CrossRef\]](#) [\[PubMed\]](#)
- Yang, D.; Huo, J. Nuclear Data Sheets for $A = 54$. *Nucl. Data Sheets* **2014**, *121*, 1–142.
- Dafni, E.; Noé, J.W.; Rafailovich, M.H.; Sprouse, G.D. Static moments of $^{54}\text{Fe}^m$ and perturbed angular distributions with combined dipole and quadrupole interactions. *Phys. Lett. B* **1978**, *76*, 51–53. [\[CrossRef\]](#)

17. Rudolph, D.; Ragnarsson, I.; Andreoiu, C.; Bentley, M.A.; Carpenter, M.P.; Charity, R.J.; Clark, R.M.; Ekman, J.; Fahlander, C.; Fallon, P.; et al. Single-particle and collective excitations in the $N = 28$ isotones ^{54}Fe and ^{53}Mn . *Phys. Rev. C* **2020**, *102*, 014316. [CrossRef]
18. Lee, I.-Y. The Gammasphere. *Nucl. Phys. A* **1990**, *520*, 641c–655c. [CrossRef]
19. Sarantites, D.G.; Reviol, W.; Chiara, C.J.; Charity, R.J.; Sobotka, L.G.; Devlin, M.; Furlotti, M.; Pechenaya, O.L.; Elson, J.; Hausladen, P.; et al. “Neutron Shell”: A high efficiency array of neutron detectors for γ -ray spectroscopic studies with Gammasphere. *Nucl. Instr. Meth. A* **2004**, *530*, 473–492. [CrossRef]
20. Sarantites, D.G.; Hua, P.-F.; Devlin, M.; Sobotka, L.G.; Elson, J.; Hood, J.T.; LaFosse, D.R.; Sarantites, J.E.; Maier, M.R. “The Microball”: Design, instrumentation and response characteristics of a 4π -multidetector exit channel-selection device for spectroscopic and reaction mechanism studies with Gammasphere. *Nucl. Instr. Meth. A* **1996**, *381*, 418–432. [CrossRef]
21. Davids, C.N.; Larson, J.D. The Argonne fragment mass analyzer. *Nucl. Instr. Meth. B* **1989**, *40–41*, 1224–1228. [CrossRef]
22. Farghaly, D. Nuclear Structure Near the Proton Drip-Line: A Search for Excited States in ^{62}Ge . Master’s Thesis, Lund University, Lund, Sweden, 2022. Available online: <https://lup.lub.lu.se/student-papers/search/publication/9085097> (accessed on 25 July 2023).
23. Böhm, P. Optimization of Gammasphere Data Following the Nuclear Reaction $^{36}\text{Ar} + ^{24}\text{Mg} \rightarrow ^{60}\text{Zn}^*$. Bachelor’s Thesis, Lund University, Lund, Sweden, 2023. Available online: <https://lup.lub.lu.se/student-papers/search/publication/9117612>. (accessed on 25 July 2023).
24. du Rietz, R.; Ekman, J.; Rudolph, D.; Fahlander, C.; Dewald, A.; Möller, O.; Saha, B.; Axiotis, M.; Bentley, M.A.; Chandler, C.; et al. Effective charges in the fp shell. *Phys. Rev. Lett.* **2004**, *93*, 222501. [CrossRef] [PubMed]

Disclaimer/Publisher’s Note: The statements, opinions and data contained in all publications are solely those of the individual author(s) and contributor(s) and not of MDPI and/or the editor(s). MDPI and/or the editor(s) disclaim responsibility for any injury to people or property resulting from any ideas, methods, instructions or products referred to in the content.